Received April 1998
Revised December 1998
Accepted January 1999

Transient conjugate heat transfer in a porous medium in concentric annuli

M.A.I. El-Shaarawi
Mechanical Engineering, King Fahd University of Petroleum and Minerals, Dhahran, Saudi Arabia
M.A. Al-Nimr
Mechanical Engineering, Jordan University of Science and Technology, Irbid, Jordan, and
M.M.K. Al Yah
Mechanical Engineering, Jordan University of Science and Technology, Irbid, Jordan

Keywords *Annuli, Forced convection, Heat transfer, Porous medium*

Abstract *Transient conjugated forced convection in the thermal entry region of a thick-walled annulus, filled with a homogeneous and isotropic porous medium, has been numerically investigated using finite-difference techniques. Non-Darcian effects as well as axial conduction of heat have been considered. The flow is assumed to be hydrodynamically fully developed and steady but thermally developing and transient. The thermal transient is initiated by a step change in the prescribed isothermal temperature on the outer surface of the external tube of the annulus while the inner surface of the internal tube is kept adiabatic. A parametric study is carried out to explore the effects of the Darcy number, the inertia term, the Peclet number and the porous medium heat capacity ratio on the transient thermal behavior in a given annulus.*

Nomenclature

a_i = radial grid size scaling factor, $(R_{i+1} - R_i)/(R_i - R_{i-1})$
a_j = axial grid size scaling factor, $(Z_{j+1} - Z_j)/(Z_j - Z_{j-1})$
C_E = Ergun coefficient, $\approx \phi/\sqrt{180\phi^5}$
c = specific heat capacity
d = pore size
Da = Darcy number, $K/(\phi r_3^2)$
h = radial thickness of any medium
J = medium parameter, = 1 for porous medium and = 2 for solid walls
k = thermal conductivity
k_e = porous medium effective thermal conductivity, $\phi k_f + (1 - \phi)k_s$
k_f = thermal conductivity of fluid
k_R = thermal conductivity ratio, K_s/k_e
k_s = thermal conductivity of the solid matrix of the porous medium
K = permeability, $-\mu$ u / (dP/dZ)
K_s = thermal conductivity of the solid walls of the annulus
l = elementary representative volume length scale
L = system length scale, = r_3 in the present case
m = number of axial increments in the numerical mesh network
n = number of radial increments inside the fluid-saturated porous medium
ns1 = number of radial increments inside the wall of the internal tube
ns2 = number of radial increments inside the wall of the external tube
N_1 = dimensionless inner radius of internal tube, r_1/r_3
N_2 = dimensionless outer radius of internal tube, r_2/r_3
N_4 = dimensionless outer radius of external tube, r_4/r_3

International Journal of Numerical Methods for Heat & Fluid Flow, Vol. 9 No. 4, 1999, pp. 444-460.

p = pressure
p_o = pressure of the fluid at channel entrance
P = dimensionless pressure, $(p - p_o)/\rho_e u_D^2$
Pe = Peclet number, $u_D r_3/\alpha_e$
Pr = effective Prandtl number, $\mu_f/\rho_f\alpha_e = \nu_f/\alpha_e$
q_w = interfacial heat flux at the interface of outer wall with fluid, $-k_e((\partial T/\partial r)_{r_3}$
Q_w = dimensionless interfacial heat flux at the interface of outer wall with fluid, $q_w/[k_e(T_o - T_w)/r_3] = (\partial\theta/\partial R)_{R=1}$
r = radial coordinate
r_1 = inner radius of internal tube
r_2 = outer radius of internal tube
r_3 = inner radius of external tube
r_4 = outer radius of external tube
R = dimensionless radial coordinate, r/r_3
Re = Reynolds number, $u_D\rho_f\sqrt{K}/\mu_f = u_D\sqrt{K}/\nu_f$
t = dimensionless time, $\tau\alpha_e/r_3^2$
T = temperature
T_{int} = interface temperature on the inner surface of the external tube of the annulus
T_M = mixing-cup (mixed-mean) temperature, $\int_{r_2}^{r_3} urTdr / \int_{r_2}^{r_3} urdr$
T_o = initial temperature
T_w = heated wall temperature
u = volume averaged axial velocity, ϕu_p
u_D = Darcian (bulk) axial velocity
u_p = pore velocity in the axial direction
U = dimensionless axial velocity, u/u_D
y = radial distance measured from the inner boundary of any medium
z = axial coordinate
Z = dimensionless axial coordinate, $z\alpha_e/(r_3^2 u_D)$

Greek symbols

α = thermal diffusivity
α_e = porous medium effective thermal diffusivity, $ke/(c\rho_f$
α_R = thermal diffusivity ratio, α_s/α_e
α_s = thermal diffusivity of solid walls
θ = dimensionless temperature, $(T - T_w)/(T_o - T_w)$
θ_{int} = dimensionless temperature on the inner surface of the external tube, $(T_{int} - T_w)/(T_o - T_w)$
θ_m = dimensionless mixing-cup (mixed-mean) temperature, $(T_M - T_o)/(T_w - T_o) = \int_{N_2}^{1} RU\theta dR / \int_{N_2}^{1} RUdR$
ρ = density
ϕ = porosity of porous medium (ratio of pore volume to total volume)
μ = dynamic viscosity
ν = kinematic viscosity, μ/ρ
τ = time
σ = heat capacity ratio of porous medium, $\phi\rho_f c_f + (1 - \phi)\rho_s c_s/(\rho_f c_f)$

Subscripts

f = fluid properties
o = initial or inlet conditions
R = ratio
s = solid properties
w = wall conditions

Introduction

Fluid flow and heat transfer in fluid-saturated porous media have a wide range of applications. Prominent among these are packed-bed chemical reactors, transpiration cooling, filtration, thermal insulation techniques, regenerative (direct-contact) heat exchangers, catalytic converters in exhaust systems of locomotive internal combustion engines, flows in soils, aquifers and petroleum extraction. In conventional heat transfer analyses, the temperature or the heat flux at the fluid-wall interface is commonly prescribed. Accordingly, the energy equation for the fluid alone can be solved to obtain the temperature field. The results obtained are therefore only good for heat transfer in flows bound by walls having extremely small thermal resistance and, in transient cases, infinitely large thermal diffusivity.

In reality, the wall thermal resistance and diffusivity are finite and hence the thermal conditions at the fluid-wall interface are different from those imposed at the outer surface of the solid wall. Consequently, the thermal conditions at

the fluid-wall interface are not known a priori and can only be obtained by solving the conjugate problem in which the heat conduction in the solid is dependent upon the convective heat transfer in the fluid and vice versa. Accordingly, the energy equations for both the solid and the fluid have to solved simultaneously.

Design calculations of heat exchangers are commonly based on steady-state heat transfer values. However, transient heat transfer information is needed for predicting the performance during start-up and shut-down periods. Moreover, to procure precise thermal control of heat exchangers one has to know their unsteady behavior. A review of the porous-media literature reveals that most of the available investigations on forced convection consider only steady-state problems, particularly flows over a flat plate and in parallel plate channels and circular tubes.

Traditional studies on porous media primarily utilize Darcian models[1,2]. The non-Darcian effects, involving inertia forces and viscous forces along the solid boundaries become more significant as the flow velocity increases or within high porosity media[3,4]. These non-Darcian effects in steady forced convection over a horizontal plate were investigated for the constant porosity case by Vafai and Tien[5], Beckermann and Viskanta[6] and Nakayama *et al.*[7,8]. Based on the Brinkman-extended flow model and for constant porosity, Kaviany[9] investigated numerically the laminar flow through a porous channel bound by two isothermal parallel plates. Vafai and Kim[10] obtained exact solutions for the velocity and temperature fields of fully developed forced convection in a porous channel bound by two parallel plates. Poulikakos and Renken[11] conducted a numerical investigation to determine the effects of flow inertia, variable porosity, and a solid boundary on fluid flow and heat transfer through porous media bound by parallel plates or in a circular pipe.

The lack of either theoretical or experimental data concerning the problem of transient conjugate heat transfer in porous annular passages motivated the present work. Transient conjugate heat transfer to a laminar forced flow with constant physical properties in the thermal entry region of a concentric porous annulus is investigated. Cooling or heating starts after steady fully developed velocity profiles are obtained and thermal transient is caused by a step change in the isothermal temperature on the outer surface of the external tube while the inner surface of the core tube is kept adiabatic.

Problem formulation

Figure 1 depicts the geometry, coordinate system and the finite-difference grid used. The geometry consists of a concentric annulus filled with homogeneous and isotropic porous medium through which a Newtonian fluid flows. The walls of the annulus are of considerable finite thickness, the porous medium is saturated with the fluid which is in local thermodynamic equilibrium with the solid matrix and both the porous medium and the walls have constant physical properties. The region under investigation begins at an axial location after the flow has become hydrodynamically fully developed; due to the presence of the

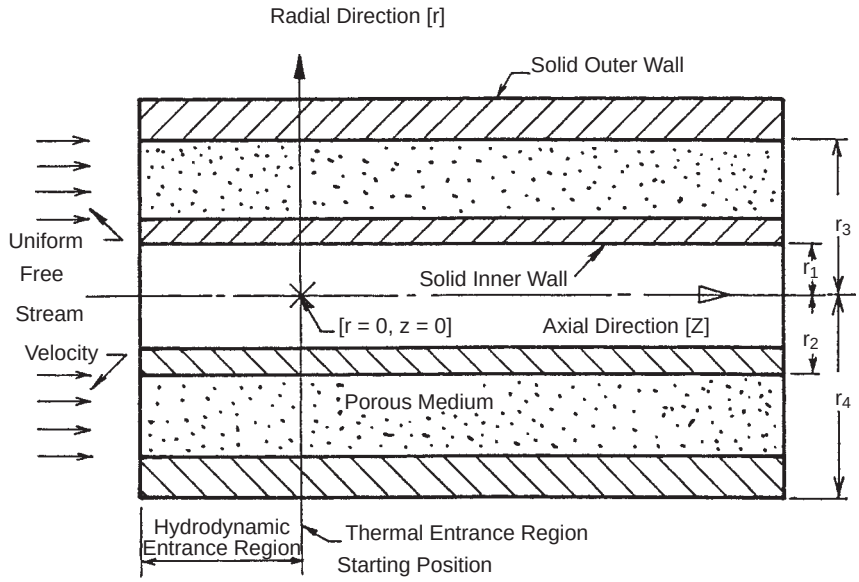

Figure 1a.
Annulus cross section and coordinate system

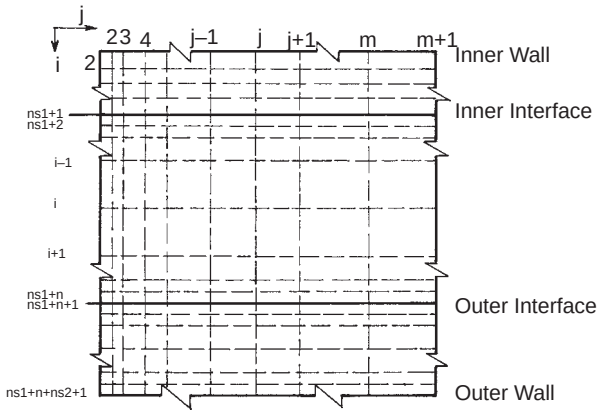

Figure 1b.
Numerical grid in R-Z plane

porous medium this location is very close to the duct entrance. Prior to the start of the step change in the temperature of the outer surface of the external tube, the fluid may either be in a thermal steady-state as a result of some previous steady-state heat transfer process, or alternately, the fluid and the annulus walls may be at the same uniform temperature, T_o. The transient conjugate heat transfer process begins at ($\tau > 0$ with a step change in the isothermal temperature of the outer surface of the external tube (from T_o to T_w) while the internal surface of the inner tube is kept adiabatic.

Assuming inertial flow regime with no internal heat generation in the fluid, the porous medium or the solid boundary walls and neglecting viscous dissipation $(2\mu(\partial u/\partial z)^2)$, the governing volume-averaged continuity, momentum and

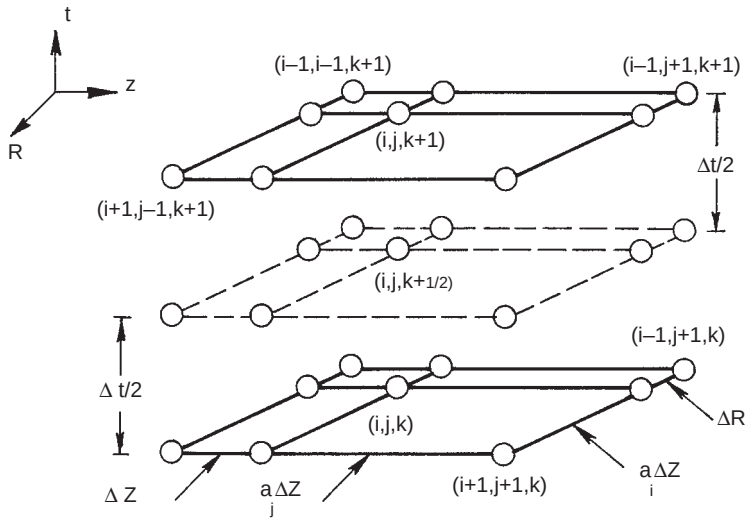

Figure 1c.
Three dimensional grid for energy equation

energy equations[4], after using the dimensionless parameters given in the nomenclature, reduce to the following non-dimensional equations, respectively:

$$\int_{N_2}^{1} RUdR = \frac{1}{2}(1 - {N_2}^2) \tag{1}$$

$$\frac{1}{R}\frac{d}{dR}R\frac{dU}{dR} - \frac{U}{Da}[1 + \mathrm{C_E\ Re\ U}] - \frac{1}{\mathrm{Pr}}\frac{dP}{dZ} = 0 \tag{2}$$

$$\sigma^{2-\mathrm{J}}\frac{\partial\theta}{\partial t} + (2-\mathrm{J})\mathrm{U}\frac{\partial\theta}{\partial Z} = (\alpha_{\mathrm{R}}^{\mathrm{J}-1}/\mathrm{R})\frac{\partial}{\partial R}\mathrm{R}\frac{\partial\theta}{\partial R} + (\alpha_{\mathrm{R}}^{\mathrm{J}-1}/\mathrm{Pe}^2)(\partial^2\theta/\partial \mathrm{Z}^2), \tag{3-4}$$

where equation (3) is obtained by setting J = 1 and is applicable for the porous medium while equation (4) is for the solid walls and is obtained by setting J = 2.

Due to the assumption of constant physical properties the energy equation, equation (3) for the fluid is not coupled to the equations for the conservation of mass and momentum (equations (1) and (2)). Thus, the hydrodynamics of the flow in the present work are independent of both the temperature and time. Therefore, the equations for the conservation of mass and momentum can be solved to determine the velocity profile U, after which the energy equations (equations (3) and (4)) can be solved, using the previously obtained U, to determine the temperature field. The initial and boundary conditions for the case under consideration are given in dimensionless forms as follows:

(1) for $\mathrm{Z} \geq 0 : \mathrm{U}(\mathrm{N}_2) = \mathrm{U}(1) = 0$ (no-slip conditions for equation 2) (5a)

(2) for $t \leq 0 : \theta_f(R, Z, t) = \theta_s(R, Z, t) = 1$ (uniform temperature everywhere) (5b)

(3) for $t > 0$ the following thermal conditions are imposed:

- at $Z = 0$ and $N_2 < R < 1 : \theta_f(R, 0, t) = 1$ (uniform temperature at the investigated-zone entrance) (5c)
- at $Z = 0$ and $N_1 < R < N_2$ and $1 < R < N_4 : \partial\theta_s/\partial Z = 0$ (5d)
- for $Z > 0$ and $R = N_2$ and $R = 1$ (solid-porous-medium interfaces): $\theta_s = \theta_f$ and $K_R(\partial\theta_s/\partial R) = \partial\theta_f/\partial R$ (continuity of heat flow) (5e)
- for $Z > 0$ and $R = N_1 : \partial\theta_s/\partial R = 0$ (adiabatic inner wall of internal tube) (5f)
- for $Z > 0$ and $R = N_4 : \theta_s(N_4, Z, t) = 0$ (step change in temperature) (5g)
- for $Z \rightarrow \infty : \partial\theta_s/\partial Z = \partial\theta_f/\partial Z = 0$ (5h)

Numerical methodology

The simultaneous hydrodynamic governing equations, equations (1) and (2) have to be solved only once, since the assumed fully-developed velocity profile U is unaffected neither by the axial location Z nor by the time t. It is worth mentioning that Kaviany[4], in his discussion on porous media velocity profiles, mentioned that "in the computations of the velocity fields, where the linear dimension of the computational domain is L, grid sizes of $0.1\sqrt{K}$ are needed to capture the boundary-layer phenomenon reasonably accurately. If a uniform mesh is used, then $l/(0.1\sqrt{K})$ nodes are needed. Noting that $L >> l > d >> \sqrt{K}$, this requirement becomes rather impossible to meet. An alternative will be variable grids ...". Therefore, to achieve economical computations and accurate results, variable grid discretization is needed in the present work. Small grid sizes are needed near the boundaries to capture sharp variations (large gradients), while large grid sizes are sufficient to reflect smooth solution variations far away from the boundaries. Indeed, porous media flow, specially in the inertial flow regime, is of uniform nature except very close to the walls that it can almost be assumed as a slip flow; when applying the no-slip conditions, a drastic change in the velocity is expected very close to the boundaries and nearly uniform flow is only present afterwards. Therefore, in solving for the velocity field, a very high stretching factor was used to compress as many nodes as possible near the boundaries. On the other hand, for the thermal field solution another variable mesh was used but with a smaller stretching factor (and hence a smaller number of grid points) since the temperature profiles do not change as drastically as the velocity near the boundaries. To achieve balance between the two fields, the obtained velocity profile was usually interpolated to fit in the new thermal domain distribution. Variable grid discretization was obtained by using the following logarithmic transformation[12] which refines the mesh near the two boundaries of every medium.

$$\bar{y} = \varepsilon + (1-\varepsilon)\,\frac{\ln(\{\lambda + [y(2\varepsilon+1)/h] - 2\varepsilon\}/\{\lambda - [y(2\varepsilon+1)/h] + 2\varepsilon\})}{\ln[(\lambda+1)/(\lambda-1)]}, \tag{6}$$

in which $\varepsilon = 0.5$ in order to refine the mesh equally near y = 0 and y = h. For this transformation, the metric $(\partial\bar{y}/\partial y)$ and the inverse transformation are, respectively, as follows

$$\frac{\partial \bar{y}}{\partial y} = \frac{2\lambda(1-\varepsilon)(2\lambda+1)}{h\{\lambda^2 - [y(2\varepsilon+1)/h - 2\varepsilon]^2\}\ln[(\lambda+1)/(\lambda-1)]} \tag{7}$$

and

$$\mathrm{y} = \mathrm{h}\,\frac{(\lambda+2\varepsilon)[(\lambda+1)/(\lambda-1)]^{(\bar{y}-\varepsilon)/(1-\varepsilon)} - \lambda + 2\varepsilon}{(2\varepsilon+1)\{1 + [(\lambda+1)/(\lambda-1)]^{(\bar{y}-\varepsilon)}/(1-\varepsilon)\}} \tag{8}$$

Thus the radial domain was discretized with finer mesh near the boundaries of each medium. A special subroutine was constructed to give different discretization modes, location of grid points and the resulting variable grid scale factors (a_i). Using the trapezoidal rule for variable grid discretization, the integral continuity equation, equation (1) can be written, after applying the no slip conditions on the two boundaries ($U_1 = U_{n+1} = 0$), as

$$\sum_{i=1}^{n} \mathrm{U_i R_i}\,\frac{a_i+1}{2}\,\Delta \mathrm{R_i} = \frac{1}{2}(1 - \mathrm{N_2}^2) \tag{9}$$

Similarly, using central differences with variable mesh sizes, the momentum equation, equation (2) can be written in the following linearized form, suitable for a simple iterative updating technique.

$$\frac{1}{R_i}\frac{U_{i+1} + (a_i^2-1)\,U_i - a_i^2\,U_{i-1}}{a_i(a_i+1)\,\Delta R_i} + 2\frac{U_{i+1} - (a_i+1)\,U_i + a_i\,U_{i-1}}{a_i(a_i+1)(\Delta R_i)^2} - \frac{1 + c_E\,Re\,U_i^*}{Da}\frac{U_{i+1} + a_i\,U_{i-1}}{a_i+1} - \frac{1}{\mathrm{Pr}}\frac{dP}{dZ} = 0$$

where U_i^* stands for the lagged velocity (from the previous iteration).

The above equation can be written as

$$\mathrm{C^*_i U_{i-1}} + \mathrm{A^*_i U_i} + \mathrm{B^*_i U_{i+1}} - \mathrm{DP} = 0, \tag{10}$$

where

$$\mathrm{C^*_i} = \frac{-a_i}{(a_i+1)\,R_i\,\Delta R_i} + \frac{2}{(a_i+1)\,\Delta R_i^2} - \frac{1 + C_E\,Re\,U_i^*}{Da}\frac{a_i}{a_i+1},$$

$$A_i^* = \frac{a_i - 1}{a_i\, R_i\, \Delta R_i} - \frac{2}{a_i\, \Delta R_i^2},$$

$$B_i^* = \frac{1}{a_i\,(a_i + 1)\, R_i\, \Delta R_i} + \frac{2}{a_i\,(a_i + 1)\,\Delta R_i^2} - \frac{1 + C_E\ \mathrm{Re}\ U_i^*}{Da}\frac{1}{a_i + 1},$$

$$\mathrm{DP} = \frac{1}{\mathrm{Pr}}\frac{dP}{dZ}, \qquad \text{and} \qquad a_i = (R_{i+1} - R_i)/(R_i - R_{i-1})$$

Excluding the Prandtl number (Pr), the present conjugate heat transfer problem is governed by nine dimensionless parameters, namely $\sigma, \alpha_R, k_R, N_1, N_2, N_4$, C_E Re, Da, and Pe. Of these nine parameters, only three (N_2, C_E Re and Da) influence the velocity field. The conventional heat transfer problems for boundary-layer flows in concentric annuli in the absence of porous media[13-15] are governed by only two parameters, namely, the Prandtl number of the fluid and the annulus radius ratio (N_2). Thus, due to the presence of the porous medium and the consideration of both the conjugated heat transfer and axial conduction of heat, eight other similarity parameters are needed to describe the problem. The Peclet number is needed due to the consideration of the axial conduction of heat ($\partial^2\theta/\partial Z^2$). To solve for the velocity field U, the values of N_2, C_E Re and Da should be selected. Then, the application of equation (10) with i = 2, 3, ..., n (i.e. in the porous medium region; with the starting values of U_i^* assumed) together with equation (9) (applied to the whole cross section) gives n linear equations in the unknown values of U_2, U_3, U_4, ..., U_n and [(dP/dZ)/Pr]. Solving these equations by means of a special form of Gauss-Jordan elimination scheme[16], one obtains the unknown values of Us and [(dP/dZ)/Pr]. Now, the obtained values of U's are fed back as updated values of U^* in the same system of equations and the iterative solution process is continued until converged values (within an acceptable tolerance) of Us and [(dP/dZ)/Pr] are obtained. In the present work, the new pressure gradient term as well as the maximum velocity component are compared with the previously obtained values. If the difference in the pressure gradient term is greater than 10^{-6} or if the maximum velocity difference is greater than 10^{-10} a new iteration is initiated. Moreover, for the cases which have studied, the matrix of coefficients pertaining to equation (10) is diagonally dominant. Accordingly, no problems have been faced on the invertibility of such matrices.

Having obtained the velocity profile U, the transient energy equations (equations (3) and (4)) can now be solved numerically. This might be done by the application of well known iterative solvers based on the preconditioned conjugate gradient method. However, in the present work, this has been done by applying central differences about the point (i, j, k+1/2), with variable grid discretization in both the R and Z directions while grid points are equally spaced in the fictitious t-direction. The ADI (Alternating-Direction Implicit) technique was used. In the ADI technique, each energy equation is replaced by

two equations (one per each half time-step, $\Delta t/2$) and each of them is implicit in only one direction and explicit in the other direction[17]. Thus, the energy equations can be replaced by the following four difference equations of which the first couple is implicit only in the R-direction while the second couple is implicit only in the Z-direction.

$$\begin{aligned} \mathrm{C_t}[\theta_{\mathrm{k+1/2}} - \theta_{\mathrm{k}}]_{\mathrm{i,j}} = {} & C_{z1}[\theta_{j+1} + (a_j^2 - 1)\theta_j - a_j^2\theta_{j-1}]_{i,k} \\ & + \mathrm{C_{z2}}[\theta_{\mathrm{j+1}} - (\mathrm{a_j} + 1)\theta_{\mathrm{j}} + \mathrm{a_j}\theta_{\mathrm{j-1}}]_{\mathrm{i,k}} \\ & + \mathrm{C_{R1}}[\theta_{\mathrm{i+1}} + (\mathrm{a_i^2} - 1)\theta_{\mathrm{i}} - \mathrm{a_i^2}\theta_{\mathrm{i-1}}]_{\mathrm{j,k+1/2}} \\ & + \mathrm{C_{R2}}[\theta_{\mathrm{i+1}} - (\mathrm{a_i} + 1)\theta_{\mathrm{i}} + \mathrm{a_i}\theta_{\mathrm{i-1}}]_{\mathrm{j,k+1/2}} \end{aligned} \tag{11-12}$$

and

$$\begin{aligned} \mathrm{C_t}[\theta_{\mathrm{k+1}} - \theta_{\mathrm{k+1/2}}]_{\mathrm{i,j}} = {} & \mathrm{C_{z1}}[\theta_{\mathrm{j+1}} + (\mathrm{a_j^2} - 1)\theta_{\mathrm{j}} - \mathrm{a_j^2}\theta_{\mathrm{j-1}}]_{\mathrm{i,k+1}} \\ & + \mathrm{C_{z2}}[\theta_{\mathrm{j+1}} - (\mathrm{a_j} + 1)\theta_{\mathrm{j}} + \mathrm{a_j}\theta_{\mathrm{j-1}}]_{\mathrm{i,k+1}} \\ & + \mathrm{C_{R1}}[\theta_{\mathrm{i+1}} + (\mathrm{a_i^2} - 1)\theta_{\mathrm{i}} - \mathrm{a_i^2}\theta_{\mathrm{i-1}}]_{\mathrm{j,k+1/2}} \\ & + \mathrm{C_{R2}}[\theta_{\mathrm{i+1}} - (\mathrm{a_i} + 1)\theta_{\mathrm{i}} + \mathrm{a_i}\theta_{\mathrm{i-1}}]_{\mathrm{j,k+1/2}} \end{aligned} \tag{13-14}$$

where

$$\mathrm{C_t} = 2\sigma^{2-\mathrm{J}}/\Delta \mathrm{t}, \mathrm{C_{z1}} = (\mathrm{J}-2)\mathrm{U_i}/[\mathrm{a_j}(\mathrm{a_j}+1)\Delta \mathrm{Z_j}],$$
$$C_{z2} = 2\alpha_R^{J-1}/[Pe^2 a_j(a_j+1)\Delta Z_j^2], C_{R1} = \alpha_R^{J-1}/[a_i(a_i+1)R_i\Delta R_i],$$
$$C_{R2} = 2\alpha_R^{J-1}/[a_i(a_i+1)\Delta R_i^2]$$

Again, the above expressions apply with J=2 for fluid and J=1 for solid walls.

The above two couples of equations can be rewritten in the following general forms:

$$\mathrm{C_i}\theta_{\mathrm{i-1,j,k+1/2}} + \mathrm{A_i}\theta_{\mathrm{i,j,k+1/2}} + \mathrm{B_i}\theta_{\mathrm{i+1,j,k+1/2}} = \mathrm{D_i} \tag{15-16}$$

where

$$\mathrm{C_i} = \mathrm{a_i^2}\mathrm{C_{R1}} - \mathrm{a_i}\mathrm{C_{R2}}, \qquad \mathrm{A_i} = \mathrm{C_t} - (\mathrm{a_i^2} - 1)\mathrm{C_{R1}} + (1 + \mathrm{a_i})\mathrm{C_{R2}},$$
$$\mathrm{B_i} = -\mathrm{C_{R1}} - \mathrm{C_{R2}}, \text{ and } \quad \mathrm{D_i} = \mathrm{C_t}\theta_{\mathrm{i,j,k}} + \mathrm{C_{z1}}[\theta_{\mathrm{j+1}} + (\mathrm{a_i^2} - 1)\theta_{\mathrm{j}} - \mathrm{a_i^2}\theta_{\mathrm{j-1}}]_{\mathrm{i,k}} +$$
$$\mathrm{C_{z2}}[\theta_{\mathrm{j+1}} - (\mathrm{a_i} + 1)\theta_{\mathrm{j}} + \mathrm{a_i}\theta_{\mathrm{j-1}}]_{\mathrm{i,k}}$$

and

$$\mathrm{C_j}\theta_{\mathrm{i,j-1,k+1}} + \mathrm{A_j}\theta_{\mathrm{i,j,k+1}} + \mathrm{B_j}\theta_{\mathrm{i,j+1,k+1}} = \mathrm{D_j} \tag{17-18}$$

where

$$C_j = a_j^2 C_{Z1} - a_j C_{Z2}, \qquad A_j = C_t - (a_j^2 - 1)C_{Z1} + (1 + a_j)C_{Z2},$$

$$B_j = -C_{Z1} - C_{Z2}, \text{ and}$$

$$D_j = C_t \theta_{i,j,k+1/2} + C_{R1}[\theta_{i+1} + (a_i^2 - 1)\theta_i - a_i^2 \theta_{i-1}]_{i,k+1/2} + C_{R2}[\theta_{i+1} - (a_i + 1)\theta_i + a_i \theta_{i-1}]_{i,k+1/2}$$

After reading the problem parameters, the first couple of equations (equations (15) and (16)) are solved for the intermediate values $\theta_{k+1/2}$. These intermediate values are then used in the second couple of equations (equations (17) and (18)), thus leading to the solution $\theta_{i,j,k+1}$ at the end of the whole time interval Δt. The coefficient matrix in both directions is tridiagonal, i.e. each couple of equations produces a system of linear equations with a tridiagonal matrix for which the Thomas method can be used to obtain the solution.

At each cross-section (i.e. a value of j), the following are used: a forward-difference representation of the boundary condition equation (5f) at i=1, the energy equation, equation (16) applied in the inner solid wall with i = 2, 3, ..., ns1, a finite-difference representation of the boundary condition equation (5e) at i=ns1+1 (i.e. at R = N_2) with a backward difference in the solid and a forward difference in the porous medium, the energy equation, equation (15) applied in the porous medium with i varies from ns1+2 until ns1+n, a finite-difference representation of boundary condition equation (5e) at i = ns1+n+1 (i.e. at R = 1) with a forward difference in the porous medium and a backward difference in the solid wall, and finally equation (16) applied in the outer solid wall with i varying from ns1+n+2 until ns1+n+ns2+1. Thus, for each value of j one obtains ns1+n+ns2+1 linear algebraic equations in the same number of unknown values of $\theta_{i,j,k+1/2}$. Thomas method, which requires low computer storage, has been used to obtain $\theta_{i,j,k+1/2}$ for each value of j, starting from j = 2 until j = m; thus, the intermediate values $\theta_{i,j,k+1/2}$ for all grid points are obtained. Now, for each i (i.e. a line of a constant value of R) equations (17) and (18) together with conditions equations (5d) and (5h) can similarly be used to obtain $\theta_{i,j,k+1}$ with j varying from 2 to m–1. Again, for each value of i, Thomas method is used to find all the unknown values of θ on this line of constant R. This is repeated for all values of i until the entire grid is again swept and hence, all the unknown values of θ at the end of the time interval Δt are obtained. The complete process of employing the two couples of difference equations in turn over successive time steps each of duration $\Delta t/2$ is then repeated so that we can advance in the time domain until steady- state conditions are reached.

Results and discussion

While computations can be performed for any combination of the nine controlling dimensionless parameters (σ, α_R, k_R, N_1, N_2, N_4, C_E Re, Da, and Pe), the objective here is to present a sample of the results that illustrate the phenomena pertinent to conjugate heat transfer and the effect of the presence of a porous medium on the transient thermal behavior of the system under

consideration. The computations were carried out for only one annular geometry of $N_1 = 0.3$, $N_2 = 0.5$ and $N_4 = 1.2$. The radius ratio 0.5 (for the porous medium region) was chosen as it represents a typical annular geometry far enough from a parallel plate channel (for which the radius ratio is unity).

The validation of the present algorithm and computer code as well as the independence of the obtained numerical results of the grid sizes were first bench-marked for relatively simple known cases, then it was checked for the present case. For example, to verify the adequacy of the numerical scheme used to obtain the velocity profile in the present work, a comparison was made at the non-porous media limit (at $Da = 10^{10}$ and CE Re = 0) with the well known fully developed annular velocity profile in concentric annuli and excellent agreement was obtained. Moreover, doubling the number of grid points did not alter the obtained velocity profile and pressure drop, although the number of iterations was slightly reduced. For more details pertaining to the verification of the adequacy of the present numerical computations and other computational aspects the reader may refer to [18].

Figures 2a and 2b clarify, respectively, the effect of Darcy number (Da) and the inertia term (C_E Re) on the velocity profile inside the annulus. As can be seen from Figure 2a, the velocity profile varies between two limits, the non-porous media regime and the slug flow regime. For a given C_E Re, as Darcy number increases (i.e. the permeability increases) the velocity profile approaches the non-porous limit. On the other hand, the slug flow limit is approached as Da decreases.

For a given Da of 10^{-3}, Figure 2b shows that the flow is attracted toward the non-porous limit as the inertia term (C_E Re) is reduced, while it becomes of more uniform nature as the inertia term is increased. This is expected since higher inertia forces mean more bulky flows. The velocity profile changes asymptotically until it reaches a certain profile near the non-porous media regime, where any reduction in the inertia term does not change the profile any

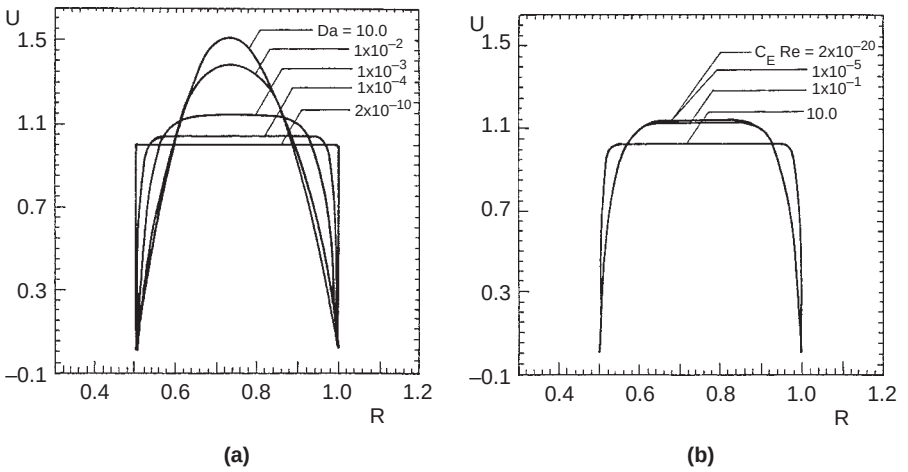

Figure 2.
(a) Effect of Darcy number on the fully-developed velocity profile, C_E Re = 2×10^8; (b) Effect of inertia term C_E Re on the fully-developed velocity profile, Da = 10^{-3}

more. Moreover, the margin of variation of the velocity profile with the inertia term is relatively small compared with that due to Darcy number. For values of $Da \leq 2\times10^{-10}$ it has been found that the effect of the inertia term (in the range of $2\times10^{-20} \leq C_E\,Re \leq 10$) is almost negligible on the velocity profile.

Thermal and control engineers are not frequently concerned with the details of the temperature profiles but only with the mixing-cup (mixed-mean or bulk) temperature (θ_m) and the wall heat flux. The practical importance of θ_m derives from its use in combination with the heat capacity and the inlet temperature of the fluid without need to obtain the local and then (by integration) the average heat transfer coefficients. On the other hand, as was explained by Faghri and Sparrow[19], the local Nusselt number in conjugate heat transfer problems include three unknowns, namely, q_w, θ_{int} and θ_m; hence it is not very informative in such conjugate cases. Instead, the interfacial heat flux distribution is usually presented.

Figure 3a gives the variation of θ_m with time at some selected axial locations (Z). Due to the step decrease in the outer surface temperature (from 1 to 0), the bulk temperature (θ_m) obviously decreases with time and similarly with Z. As can be seen from this figure, as the time decreases, curves corresponding to different values of Z separate from the conduction envelope. In other words, a curve corresponding to a given Z separates from the conduction envelope at the time of onset of convection; before this time the heat is transferred from the boundary wall to the porous medium solely by conduction. Indeed, the time needed for the onset of convection (i.e. the point of separation from the pure conduction envelope) increases with Z. On the pure conduction envelope, the fluid velocity is too large so that the fluid reaches a cross-section under consideration (i.e. a value of Z) before the radial heat diffusion signal coming from the suddenly heated outer wall of the annulus. On the other hand, for a given value of Z, θ_m continues its development with time until steady-state conditions are reached (without further variation in θ_m; the time required to reach the steady-state value of θ_m is proportional to the axial location. As $Z\rightarrow\infty$ and $t\rightarrow\infty$, θ_m can asymptotically approach the outer wall temperature ($\theta_m = 0$) if there were no outer-wall thermal resistance.

Figure 3b shows, for the same conditions and axial locations of Figure 3a, the transient variation of the interfacial outer-wall temperature with time. A horizontal line of zero value represents the no-wall conduction case. Thus, it can be concluded from this figure that neither at the beginning of the time domain nor near the entrance cross-section ($Z = 0$), the temperature profiles are close to the no-wall heat transfer line. Consequently, the consideration of conjugated heat transfer is of great importance near the channel entrance and at the start of the transient heat transfer process. The variation of the interfacial wall heat flux with time is presented in Figure 3c for the same conditions as used to develop Figures 3a and 3b. In light of the previous discussion on Figures 3a and 3b, the results of Figure 3c are self-explanatory.

For given values of the other eight controlling parameters (N_1, N_2, N_4 C_E Re, Da, σ, α_R and k_R), Figures 4a-c present the effect of Peclet number (Pe) on the

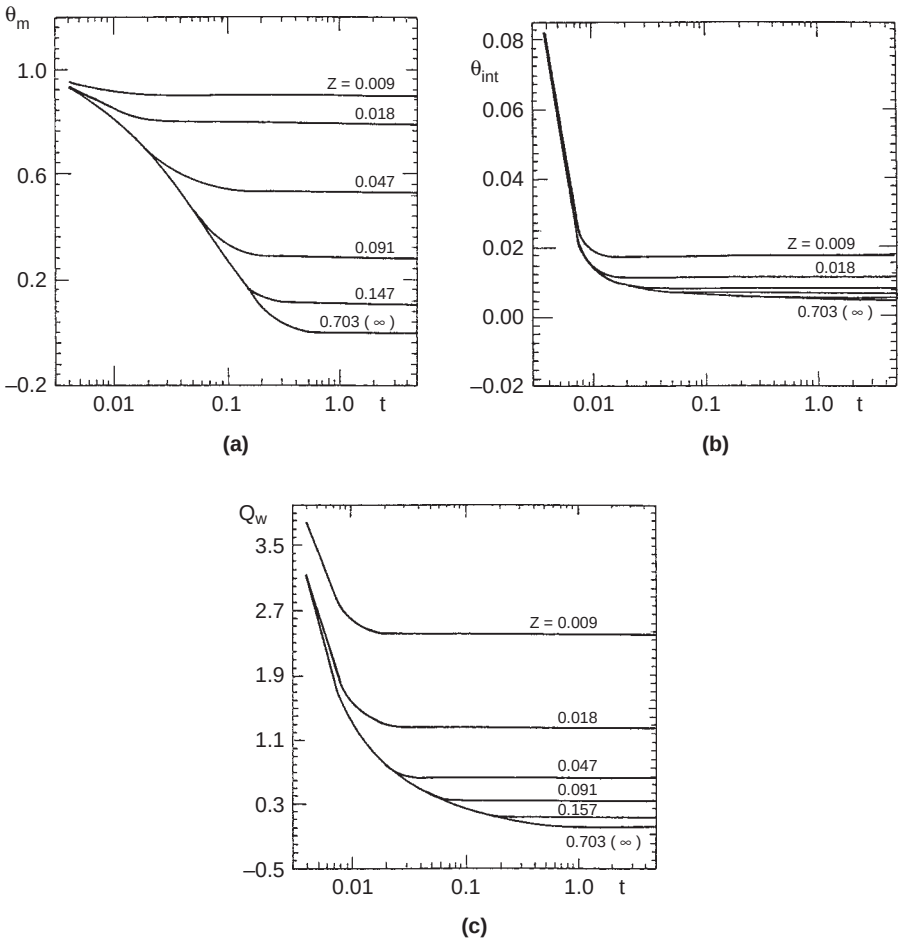

Figure 3.
Variation with time of: (a) θ_m, (b) θ_{int} and (c) Q_w for different values of Z, Da = 2×10^{-10}, C_E Re = 2×10^{-8}, $\sigma = 0.5$, $\sigma_R = 100$, $K_R = 150$, Pe = 10^8

interfacial wall heat flux (Qw). For a considerably large value of t (t= 5×10^{-3}), Figure 4a gives the curves of the variation of Q_w with axial distance (Z) corresponding to some selected values of Pe while Figure 4b gives these curves for a very small value of t (t = 9×10^{-5}, i.e. just after the thermal transient starts). It is evident from Figure 4a that the smaller the value of Pe the higher the value of Qw and the larger the thermal entrance length. This is because the lower the value of Pe the slower the development of the thermal boundary layer. However, as can be seen from Figure 4a, the curve corresponding to Pe = 120 is very close to that corresponding to Pe = ∞. In other words, from the presented results, it is concluded that for Pe greater than about 120 the axial conduction of heat ($\partial^2\theta/\partial Z^2$) can be assumed negligible provided that the value of the time (t) is large. For very small values of t and particularly very near to the entrance (i.e. small values of Z), neglecting the axial conduction is not a valid assumption as can be observed from Figure 4b. Accordingly, axial

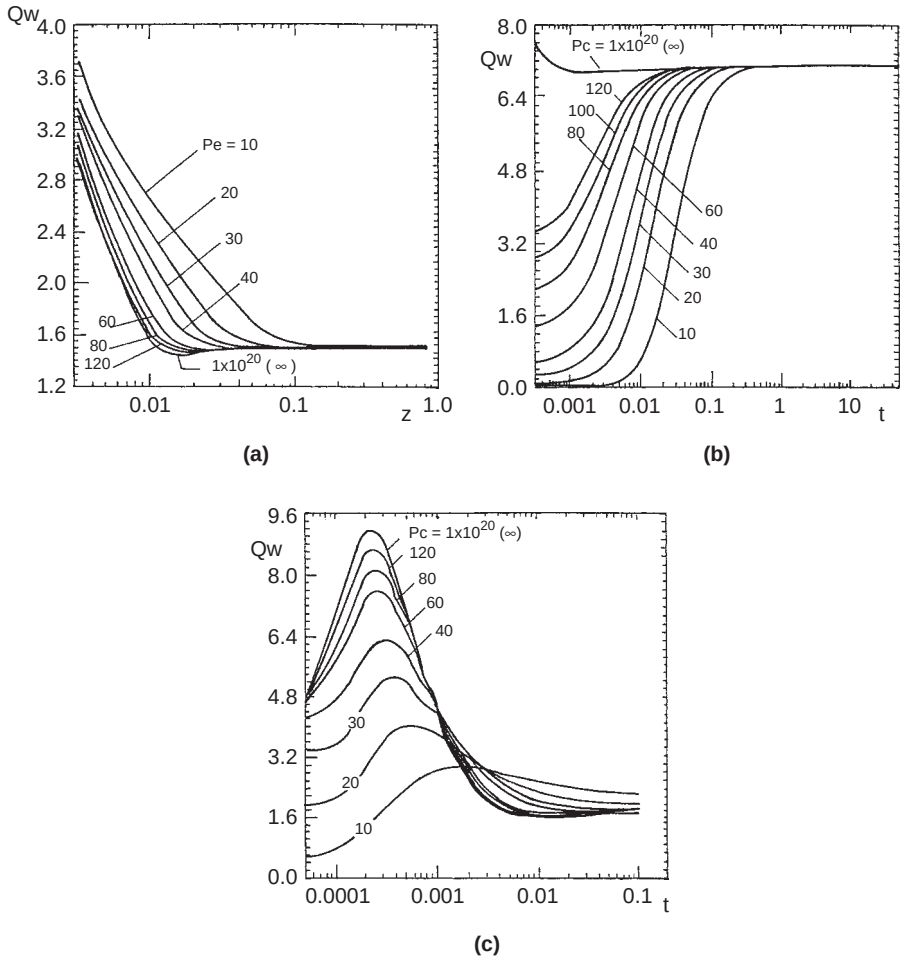

Figure 4.
Effect of Pe on interfacial wall heat flux (Q_w), Da = 2×10^{-10}, C_E Re = 2×10^{-8}, σ = 0.5, α_R = 100, K_R = 150, Pe = 10^8; (a) Q_w versus Z for considerably large value of t (t = 0.005), (b) Q_w versus Z for very small value of t (t = 9×10^{-5}), (c) Q_w versus t for Z = 0.009

conduction can never be overlooked for very small values of the time (close to the moment of initiation of the thermal transient); the effect of axial conduction decays as the time elapses provided that Pe is very large ($\geq$ 120).

For a given Z, Figure 4c presents the variation of the interfacial heat flux (Q_w) with time for the selected values of Pe as a parameter. It can be seen that, for each value of Pe, there exists a peak for Q_w. This peak represents the end point of the thermal lag of the system due to the thermal resistance of the wall (wall thickness effect). A careful scrutiny of this figure reveals the effect of axial conduction on heat transfer to/from the porous medium. For the no-wall conduction limit, i.e. Pe $\rightarrow \infty$, the peak is sharp and steady state is reached relatively early. As the axial conduction influence increases (i.e. Pe decreases), the peak is flattened and slightly shifted forward, yielding a longer transition period. The shorter time required to reach the steady state at high values of Pe is

due to the fact that the thermal energy in the heated wall of the annulus is carried away downstream by the porous medium and its flowing fluid without having backward conduction in either the porous medium or the walls of the annulus.

Figures 5a and 5b clarify the effect of the porous medium thermal capacity ratio (σ) on the interfacial outer-wall heat flux. For a given time (t), Figure 5a gives the variation of Q_w with Z for various selected values of σ. As can be seen from this figure, increasing the value of σ increases Q_w, particularly after some distance from the entrance, and the thermal entrance length becomes shorter. This is attributed to the higher radial conduction to/from the solid matrix of the porous medium as σ increases and to the domination of convection very near to the entrance while conduction becomes a pronounced means of heat transfer further downstream. Recall that higher values of σ imply more solid matrix material within the porous medium. Figure 5b provides, for a given Z, the transient variation of Q_w for various values of σ. As σ increases both Q_w and the time required to reach steady state increase. The effect of σ on Q_w is less pronounced as the steady-state conditions are approached.

The effect of Darcy number (Da) on the interfacial outer-wall heat flux is given in Figure 6. For a given time, Figure 6 gives the axial variations of Q_w for some selected values of Da. For a given Z, decreasing Da causes an increase in the value of Q_w. This is attributed to the fact that as Da decreases, the inertia forces become more pronounced and hence the fluid becomes more capable of carrying thermal energy downstream (i.e. Q_w increases).

For a given Z, Figure 7 demonstrates the transient variation of the interfacial wall heat flux for various values of the inertia term C_E Re. This figure shows that increasing the inertia term increases the interfacial wall heat flux. This is anticipated since larger values of C_E Re imply higher velocities and hence higher values of heat transfer.

Finally, it might be noteworthy that no results have been presented for the effect of wall-to-porous-medium thermal diffusivity ratio (α_R) and thermal

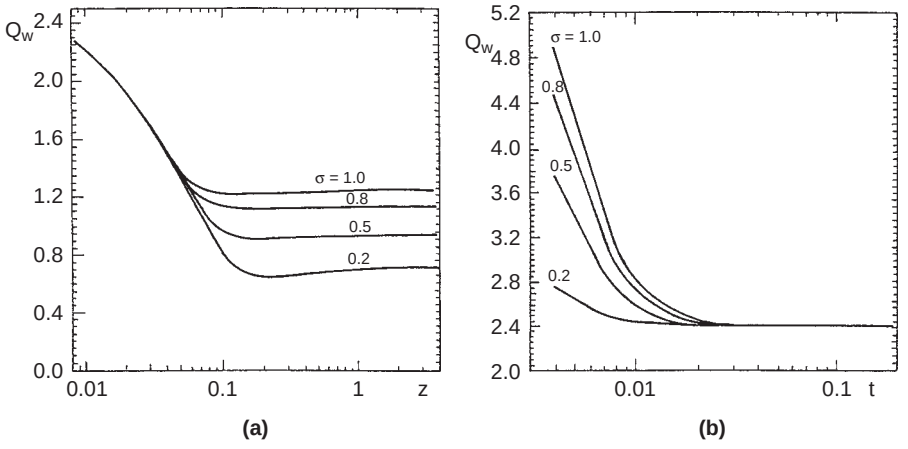

Figure 5.
Effect of porous medium thermal capacity ratio (σ) on the interfacial wall heat flux (Q_w), Da = 2×10^{-10}, C_E Re = 2×10^{-8}, σ = 0.5, α_R = 100, K_R = 150, Pe = 10^8; (a) Q_w versus Z for t = 0.075, and (b) Q_w versus t for Z = 0.009

conductivity ratio (K_R). Indeed, this is due to space limitations and because the pertinent results are qualitatively similar to those previously known in the literature; in this regard the reader may refer to a recent publication[20].

Conclusions

Transient conjugated forced convection in the thermal entry region of a thick-walled annulus, filled with an isotropic and homogeneous porous medium, has been numerically investigated. The thermal transient has been obtained due to a sudden change in the outer surface temperature of the external tube. The axial conduction in both the porous medium and the thick walls of the annulus have been considered. It has been found that the axial conduction can be neglected for Peclet number greater than 120. Darcian and non-Darcian effects have been considered in the investigation and a parametric study has shown the following. Both the Darcy number and the inertia term have influence on the fully developed velocity profile and consequently on the heat transfer to the porous medium. Increasing the porous medium thermal capacity ratio increases the heat transfer and reduces the thermal entrance length.

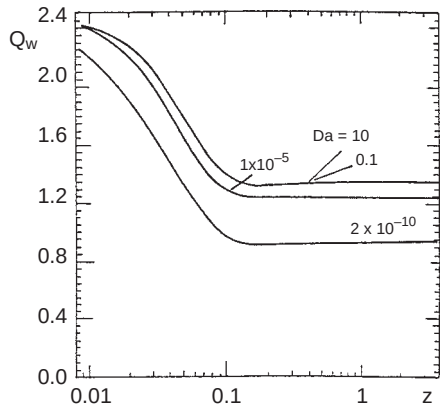

Figure 6.
Effect of Darcy number on variation of Q_w with Z, t = 0.075, C_E Re = 2×10^{-8}, α_R = 100, K_R = 150, Pe = 10^8

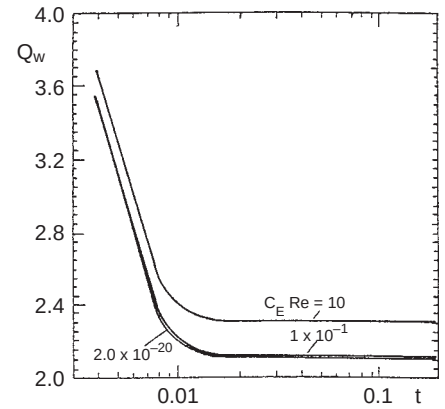

Figure 7.
Effect of the inertia term C_E Re on the transient variation of Q_w, Z= 0.009, Da = 10^{-3}, σ = 0.5, α_R = 100, K_R = 150, Pe = 10^8

References

1. Bejan, A., *Convection Heat Transfer*, John Wiley and Sons, New York, NY, 1984.
2. Nakayama, A. and Pop, I., "A uniform similarity transformation for free, forced and mixed convection in Darcy and non-Darcy porous media", *Int. J. Heat Mass Transfer*, Vol. 34, 1991, pp. 357-567.
3. Palm, A., Weber, J.E. and Kvernold, O., "On steady convection in a porous medium", *J. Fluid Mechanics*, Vol. 54, 1972, pp. 153-61.
4. Kaviany, M., *Principles of Heat Transfer in Porous Media*, Springler-Verlag, New York, NY, 1991.
5. Vafai, K. and Tien, C.L., "Boundary and inertia effects on flow and heat transfer in porous media", *Int. J. Heat Mass Transfer*, Vol. 24, 1981, pp. 195-203.
6. Beckermann, C. and Viskanta, R., "Forced convection boundary-layer flow and heat transfer along a flat plate embedded in a porous medium", *Int. J. Heat Mass Transfer*, Vol. 30, 1987, pp. 1547-51.
7. Nakayama, A., Koyama, H. and Kuwahara, T., "Analysis on forced convection in a channel filled with a Brinkman-Darcy porous media-exact and approximate solutions", *Warme und- Stoffubertrag*, Vol. 23, 1988, pp. 291-5.
8. Nakayama, A., Kokudai , T. and Koyama, H., "Non-Darcian boundary layer flow and forced convection heat transfer over a flat plate in a fluid-saturated porous medium", *J. Heat Transfer*, Vol. 112, 1990, pp. 157-62.
9. Kaviany, M., "Laminar flow through a porous channel bounded by isothermal parallel plates", *Int. J. Heat Mass Transfer*, Vol. 28, 1985, pp. 851-8.
10. Vafai, K. and Kim, S.J., "Forced convection in a channel filled with a porous medium; an exact solution", *J. Heat Transfer*, Vol. 111, 1989, pp. 1103-6.
11. Poulikakos, D. and Renken, K., "Forced convection in a channel filled with a porous medium including the effect of flow inertia variable and Brinkman friction", *J. Heat Transfer*, Vol. 109, 1987, pp. 880-8.
12. Anderson, D.A., Tannehill, J.C. and Pletcher, R.H., *Computational Fluid Mechanics and Heat Transfer*, Hemisphere Publishing Co., New York, NY, 1984.
13. Coney, J.E.R. and El-Shaarawi, M.A.I., "Finite difference analysis for laminar flow heat transfer in concentric annuli with simultaneously developing hydrodynamic and thermal boundary layers", *Int. J. Numerical Methods Engng*, Vol. 9, 1975, pp. 17-38.
14. El-Shaarawi, M.A.I. and Sarhan, A., "Free convection effects on the developing laminar flow in vertical concentric annuli", *J. Heat Transfer*, Vol. 102, 1980, pp. 617-22.
15. El-Shaarawi, M.A.I. and Alkam, M.K., "Transient forced convection in the entrance region of concentric annuli", *Int. J. Heat Mass Transfer*, Vol. 35, 1992, pp. 3335-44.
16. El-Shaarawi, M.A.I., "Heat transfer and hydrodynamics in the entrance region of concentric annuli with stationary and rotating inner walls", PhD Thesis, The University of Leeds, Leeds, UK, 1974.
17. Carnahan, B., Luther, H.A. and Wilkes, J.O., *Applied Numerical Methods*, Wiley, New York, NY, 1969.
18. Alyah, Mua'ath M.K.Y., "Transient conjugated heat transfer in the developing region of a porous concentric annulus", MS Thesis, Jordan University of Science and Technology, Irbid, Jordan,1988.
19. Faghri, M. and Sparrow, E.M., "Simultaneous wall and fluid axial conduction in laminar pipe-flow heat transfer", *J. Heat Transfer*, Vol. 102, 1980, pp. 58-63.
20. El-Shaarawi, M.A.I., Al-Nimr, M.A. and Hader, M.A., "Transient conjugated heat transfer in concentric annuli", *Int. J. Num. Meth. Heat Fluid Flow*, Vol. 5, 1995, pp. 459-73.